



HAL
open science

Biodetection of DNA and proteins using enhanced UV absorption by structuration of the chip surface

Kristelle Robin, Jean-Luc Reverchon, Laurent Mugerli, Michel Fromant,
Henri Benisty

► **To cite this version:**

Kristelle Robin, Jean-Luc Reverchon, Laurent Mugerli, Michel Fromant, Henri Benisty. Biodetection of DNA and proteins using enhanced UV absorption by structuration of the chip surface. SPIE Photonics West, Jan 2009, San Jose, United States. pp.718804, 10.1117/12.808124 . hal-00573363

HAL Id: hal-00573363

<https://hal.science/hal-00573363>

Submitted on 24 Aug 2022

HAL is a multi-disciplinary open access archive for the deposit and dissemination of scientific research documents, whether they are published or not. The documents may come from teaching and research institutions in France or abroad, or from public or private research centers.

L'archive ouverte pluridisciplinaire **HAL**, est destinée au dépôt et à la diffusion de documents scientifiques de niveau recherche, publiés ou non, émanant des établissements d'enseignement et de recherche français ou étrangers, des laboratoires publics ou privés.



Distributed under a Creative Commons Attribution 4.0 International License

Biodetection of DNA and proteins using enhanced UV absorption by structuration of the chip surface

K. Robin^{a*}, J. L. Reverchon^a, L. Mugerli^b, M. Fromant^b and H. Benisty^c

^aThales Research and Technology, RD 128, 91767 Palaiseau Cedex, France

^bLaboratoire de Biochimie, Ecole Polytechnique, CNRS, 91128 Palaiseau Cedex, France

^cLaboratoire Charles Fabry de l'Institut d'Optique, CNRS, RD 128, 91127 Palaiseau Cedex, France

e-mail: kristelle.robin@thalesgroup.com

ABSTRACT:

DNA and protein absorption at 260 and 280 nm can be used to reveal these species on a biochip UV image. A first study including the design and fabrication of UV reflective multilayer biochips designed for UV contrast enhancement (factor of 4.0) together with spectrally selective AlGaIn detectors demonstrated the control of chip biological coating, or Antigen/Antibody complexation with fairly good signals for typical probe density of 4×10^{12} molecules/cm².

Detection of fractional monolayer molecular binding requires a higher contrast enhancement which can be obtained with structured chips. Grating structures enable, at resonance, a confinement of light at the biochip surface, and thus a large interaction between the biological molecule and the lightwave field. The highest sensitivity obtained with grating-based biochip usually concerns a resonance shift, in wavelength or diffraction angle. Diffraction efficiency is also affected by UV absorption, due to enhanced light-matter interaction, and this mechanism is equally able to produce biochip images in parallel.

By adjusting grating parameters, we will see how a biochip that is highly sensitive to UV absorption at its surface can be obtained. Based on the Ewald construction and diffraction diagram, instrumental resolution and smarter experimental configurations are considered. Notably, in conjunction with the 2D UV-sensitive detectors recently developed in-house, we discuss the obtainment of large contrast and good signals in a diffraction order emerging around the sample normal.

Keywords: Label-free biosensors; Enhanced optical absorption; Absorption imaging; Ultraviolet spectrally selective AlGaIn components.

1. INTRODUCTION

This work takes part of an innovative label-free optical detection method: UV imaging of biochips. This method exploits DNA and protein absorption, respectively at 260 nm and 280 nm. To be sensitive, our detection method requires the use of contrast enhancing biochips. This paper describes the design of reflective biochips, which will enhance the absorption contrast when a thin biological layer is located on their surface. The basic idea of these biochip is to enhance the interaction between the biological molecules and the wave electric field, and thus to increase the absorption-induced contrast. Multilayer biochips have first been recently developed by us, and showed a sensitivity sufficient to detect an absorption $\alpha \ell$ in the 10^{-3} order (biological monolayer absorption). To be able to detect sub-monolayer molecular binding events in typical biological “spot” sizes ($\sim 100 \mu\text{m}$), we use coupling properties of light with matter by designing structured biochips.

*kristelle.robin@thalesgroup.com

2. LABEL-FREE BIODETECTION BASED ON ULTRAVIOLET IMAGING

2.1 Label-free optical biosensors

Biosensors are devices used to detect target biological molecules. They comprise of a biological element linked to a transducer which converts the biological recognition into a measurable signal. The transducer can be of variable nature and there is a wide large interest in detection methods which do not require labeling of molecules (because labels such as particles, fluorophores, quantum dots may influence the biochemical binding processes). The detection method we propose here is a label-free imaging method based on an intrinsic property of biological molecules: UV absorption.

Label-free optical detection methods can be divided into two groups: reflectometric and refractometric methods (Ref. [[1]]). Reflectometry has been introduced based on ellipsometry to characterize thin layers many decades ago. The need of polarized radiation can be circumvented by using multipath reflection at thin layer interfaces (as is done in reflectometric interference spectroscopy, RIfS). This is based on principles of Fabry-Perot interferometry, either with multi- or single wavelength radiation. Refractometric methods use the change in the refractive index at a chip surface. Since surface plasmon resonance has been commercialized, it is a reference method which has lead to far more publications than grating couplers, resonant mirrors or Mach-Zehnder interferometry, among the possible principles applicable to biosensors. However, refractometric methods need better referencing because of the temperature dependency of the refractive index.

DNA and proteins absorb UV light respectively at 260 nm and 280 nm. The absorption signal can also be used to image biochips with a transmission or reflection set-up (in general decrease of the reflectivity). To provide a good sensitivity and minimize UV illumination, the optical contrast has to be enhanced. This is realized using contrast-enhancing biochip, either multilayer biochips or structured biochip. The design and fabrication of these chips will be presented in this paper. UV absorption is currently used by biologists to determine concentration of DNA or proteins in solution, and has consequently tabulated values. Moreover, it is less sensitive to temperature changes (imaginary part of the optical index) in comparison to method based on the change of the real part of the refractive index on the chip surface.

2.2 Absorption of DNA and proteins in UV

2.2.1 Absorption in solution: Beer-Lambert law

To have a better insight in the absorption strength that we have to detect, we start here with an evaluation of DNA and protein absorption. The absorbance A_λ is given by the Beer-Lambert law:

$$A_\lambda = -\log\left(\frac{I_\lambda}{I_{\lambda o}}\right) = \varepsilon_\lambda \ell c, \quad (1)$$

with c the mass concentration in $\mu\text{g}/\text{cm}^3$, l the path length in cm, $I_{\lambda o}$ and I_λ the intensities without and with absorber. ε_λ the mass extinction coefficient at the wavelength λ in $\text{cm}^2/\mu\text{g}$. Considering $\ell = 1\text{cm}$, we can express A_λ as a surface absorption related to the mass surface density ℓc

2.2.2 Protein absorption

For a similar mass coverage and taking into account amino acids abundance in nature, protein absorption is roughly one order of magnitude smaller than that of DNA. This is the reason why in this paper, we will mainly deal with protein absorption. However, the absorption sensitivity obtained for proteins would a fortiori be valid for DNA.

Proteins start to absorb UV light in proportion to their aromatic amino acids content (Tryptophan, Tyrosine and Phenylalanine). This absorption peaks at $\lambda=280$ nm. In figure 1(a), we give the absorption spectrum of an *Escherichia coli* histidine-tagged methionyl-tRNA synthetase (MetRS) protein (20 mM potassium phosphate buffer, pH 8.5). The MetRS protein, whose mass extinction coefficient $\varepsilon_{280\text{nm}}$ is $1.72 \times 10^{-3} \text{ cm}^2/\mu\text{g}$ [[3]] is used in the experiments presented in this paper. For typical probe density of 4×10^{12} molecules/ cm^2 , it corresponds to an absorption in transmission $\alpha \ell \cong A_{280\text{nm}} = 0.73 \times 10^{-3}$.

The UV absorption spectrum of relevant species are superimposed to the emission spectrum of AlGaN detectors (dash-dotted line) [[4]] and of recently developed UV LED [[5]] (dotted line). The biological absorption spectral width is 10 nm or so. The use of spectrally selective AlGaN detectors and/or UV LED consequently fits well our applications. In the following subsection, we give a brief inventory of UV sources and detectors, which have recently witnessed a growing interest.

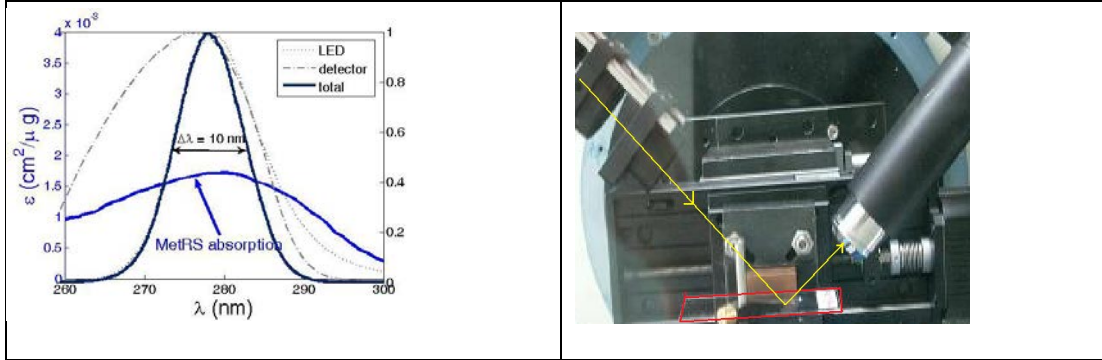


Fig 1. : (a) MetRS protein absorption spectrum superposed to a deep UV LED emission spectrum ($\lambda_{\max} = 280 \text{ nm}$, $\Delta\lambda=12\text{nm}$) and to the sensitivity spectrum of our AlGaN detector ($\lambda_{\max} = 278 \text{ nm}$, $\Delta\lambda=20\text{nm}$). The instrumental spectral characteristics (λ_{\max} and $\Delta\lambda$) fits the absorption spectrum of proteins well. (b) Experimental set-up used to image biochips.

2.3 UV sources and detectors

2.3.1 Detection

Since the development of Wood's glass, UV imaging has known a constant but always confidential use. Different kinds of camera more or less adapted to UV wavelengths have been developed. When thinned, CCD [[6]] have the capability to present large quantum efficiency in ultraviolet. Such devices have been developed for space applications and are now largely used in spectroscopy or microscopy. Photon counting based on electron multiplication (EM) in registers can also be achieved with EMCCD when it is cooled down to 200K. Hybrid CMOS technologies [[7]] have also been adapted to reach an enhanced quantum efficiency exceeding 40% in the spectral range from 300nm to 400nm. It consists of a readout circuit hybridized to a 2D array of photodiodes presenting a 100% filling factor. The latest approach exploits back-thinned CMOS monolithic imagers less prone to irradiation damage [[8]]. Nevertheless, some applications like solar-blind detection need to extract extremely low fluxes immersed in a strong visible light and rejection of visible light is a challenge. In this case, the spectral selectivity of photo-cathodes associated to filters with a sharp visible rejection of solar illumination has been successfully employed in U.V. detection [[9]].

Nevertheless, UV imaging is not yet developed, notably due to the rather poor specifications of UV filters. Even with a long experience, such filters are not so friendly to use to the desired requirements. Consequently, use of an AlGaN array associated to a hybrid CMOS multiplexer is probably one of the best ways to replace photocathodes and achieve UV solar blind detector. AlGaN hybrid CMOS is an extension of hybrid-CMOS we have developed for several years. It can also achieve large quantum efficiency, low electrical noise and advanced functionalities in image processing. Use of an AlGaN array associated to an hybrid CMOS multiplexer is probably one of the best ways to replace photocathodes. Moreover hetero-structures based on different aluminum contents in the constituting alloys provide tunable band pass filtering of 10 to 20nm. This naturally prevents the spurious effects of chromatic aberration due to the huge index dispersion taking place in the ultraviolet range, even for UV compatible materials.

2.3.2 Sources

Wide and direct energy band of III-Nitride semiconductors make this material system uniquely suited for fabrication of light emitting devices (LEDs and Lasers) with peak emission wavelengths in UV spectral range from 365 nm to 255nm. Recently, significant improvements in materials quality and device design resulted in demonstration of light emitting diodes (LEDs) capable to deliver tens of mW cw powers in 260-365 nm wavelength range [[10]]. Even if AlGaIn Laser diodes are currently available for blue ray, few devices have been developed below 360nm. The remaining solutions are based on non-linear crystals assisted with solid-state diode-pumped lasers such as those proposed by several companies [[5]].

2.3.3 Imaging set-up

In figure 1(c), a picture of our imaging set-up is given. The sample is illuminated with a UV source. Here the source is a UV LED ($\lambda_{\max} = 280$ nm, $\Delta\lambda = 12$ nm). The reflected signal is measured using an AlGaIn spectrally selective detector ($\lambda_{\max} = 278$ nm, $\Delta\lambda=20$ nm) and we are then insensitive to visible illumination. The position of the source and the detector depend on the configuration used. If the specular reflection is measured, a $\theta=0$ configuration is used. Concerning structured biochips, depending on the diffraction order being measured, the detector is placed in the corresponding diffracted angle.

2.4 Reflectivity induced contrast

Considering a thin absorbing layer of absorbing coefficient α and of thickness ℓ on a reflective multilayer chip of reflectivity R_{chip} , the absorption induced contrast C is defined by:

$$C = -\frac{\Delta R}{R_{chip}} = -\frac{R_{chip} - R_{protein}}{R_{chip}} > 0 \quad (2)$$

The contrast enhancement $\Gamma = C/\alpha\ell$ is the ratio of the reflectivity induced contrast and the absorption in transmission $\alpha\ell$. A monolayer of proteins of typical probe density of 4×10^{12} molecules/cm² corresponds to an absorption in the 10^{-3} order. To be able to detect this weak absorption signal or even lower contrast (detection of fractional monolayer molecular binding), the contrast has to be enhanced. Note that the limit $R_{chip} \rightarrow 0$ apparently boosts the quantity C, but the signal-to-noise ratio is generally weak in this case. Hence we will assume that R_{chip} retains a sizable value.

In this paper, we present the design and fabrication of contrast enhancing biochip. Basically, they are designed to maximize the interaction between the electromagnetic field and the absorbing layer, and consequently to enhance the reflectivity induced contrast. In this paper, we first present imaging results obtained with multilayer biochips, which enables a contrast enhancement of a factor 4.0. Then, to achieve a more sensitive detection system, we design structured biochip. The design and characteristics of these biochips are described, both theoretically and experimentally, by characterizing their angular reflectivity.

3. MULTILAYER BIOCHIPS IMAGING

3.1 Theory

The biochip used is a UV reflective multilayer structure. In the imaging experiment, it consists in an aluminum mirror covered with silica of index $n=1.495$ at $\lambda=280$ nm. Silica is chosen for transparency of the material and for biocompatibility. Moreover, the oxygen bonds are required for our biological coating process (see subsection 3.2). Silica thickness is chosen to maximize the interaction of the electric field with the biological molecules. Indeed, by choosing a quarter-wave optical thickness of silica, the absorbing layer on the chip surface is located at antinode of the standing wave electric field and the interaction is maximized. The electric field amplitude on the interface is of $1+\sqrt{R}$, with R close from unity for a mirror. Fine modelling of a fabricated multilayer biochip composed of quarter-wave PECVD silica deposit on an aluminium mirror gave a reflectivity value of $R = 0.72$. For non-polarized light, absorption contrast is enhanced by a factor of 4.0 (see [[11]] and more particularly the note in this paper about the exploitation of its ref 13, Benisty et al, 1998).

3.2 Experimental results

3.2.1 Chip fabrication and preparation

To fabricate our silica on aluminum biochip, a silicon substrate was first sputtered with aluminum, and then covered with a quarter-wave thickness silica layer deposited by PECVD at 340°C. In order to make biological spots of typical size 100 μm , the chip was covered with a SPR 220 positive photoresist (Shipley) before activation with an Ar/O₂ plasma and chemical vapor deposition of 3-aldehydopropyltrimethoxysilane. The photoresist was then removed with acetone, leaving aldehyde functionalised spots, which will react readily with the MetRS protein amino groups during incubation phase. Then, some of the slides are incubated with specific and non-specific antibodies, to validate the specificity of our imaging technique. Figure 2 gives a scheme of our biochip. With quarter-wave silica thickness, the biological layer is located at the antinode of the electric field and the interaction is maximized.

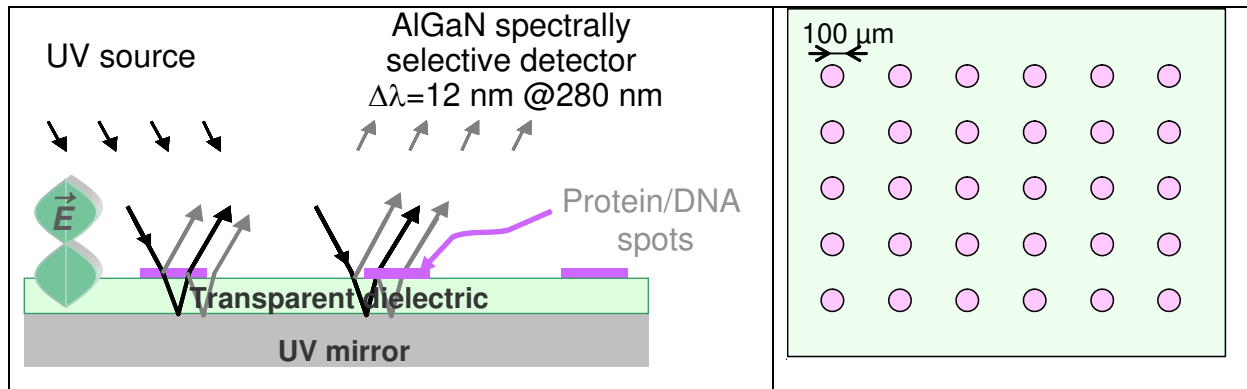


Fig. 2: Side view and top view of the fabricated biochip, composed of a quarter-wave silica layer on an aluminum mirror.

3.2.2 Biochip imaging

With a contrast enhancement of 4.0 and taking into account instrumental noise contributions, the sensitivity is already sufficient to image a biochip covered with a monolayer of proteins (typically 4×10^{12} molecules/cm²), of absorption in the few 10^{-3} order. We give here experimental results obtained with multilayer biochips composed on a quarter-wave silica layer on an aluminium mirror.

Figure 3(a) gives a UV image of a biochip coated with the MetRS protein. This validates a possibly useful application such as coating control. On the absorption profile given in figure xx(c), the measured absorption is of $4.9 \pm 0.3 \times 10^{-3}$. For monolayer coverage of density 4×10^{12} molecules/cm², corresponding to a volume per protein of $5 \times 5 \times 10 \text{ nm}^3$ (volume of MetRS in solution) the calculated reflectivity decrease expected is $\Delta R = 4.0 \times A_{280 \text{ nm}}, R = 2.1 \times 10^{-3}$. The somewhat higher absorption can be explained by a larger than expected protein density, and by optical effects such as scattering due to roughness and optical index contrast. Next, the specificity of our biosensing technique was validated by incubating the MetRS-coated biochip with specific and non-specific antibodies. In figure xx(b), we give an image of a chip coated with MetRS after specific recognition of a specific antibody. On the UV image, we measure absorption after complexation of $7.9 \pm 0.5 \times 10^{-3}$. Assuming that roughness of the surface and optical index contrast are similar before and after complexation, the measured absorption increase $\Delta A = 3 \pm 0.6 \times 10^{-3}$ upon antibody complexation can be attributed to the absorption of the antiHis-Ab molecules specifically linked to the MetRS molecules. It corresponds to a surface density of $2.8 \pm 0.5 \times 10^{12}$ molecules/cm². This value is close from a densely packed IgG monolayer, and explains why a 1:1 MetRS/Ab stoichiometry can not be reached.

On the contrary, no absorption increase was measured for the biochip incubated with a non-specific anti-mouse IgG Horseradish-Peroxidase-linked whole antibody (Amersham Biosciences, 1/2000), which means that these antibodies do not link nonspecifically with the MetRS proteins and validates the specificity of our biosensing technique.

However, with these biochips, our system is not sufficiently sensitive for detection of fewer events (even if 1 μm^2 can be imaged, it still represents 4×10^4 proteins). Consequently, a structuration of the chip surface is carried out to confine the electric field at the chip surface, where the biological element is located and therefore to maximize the absorption induced contrast.

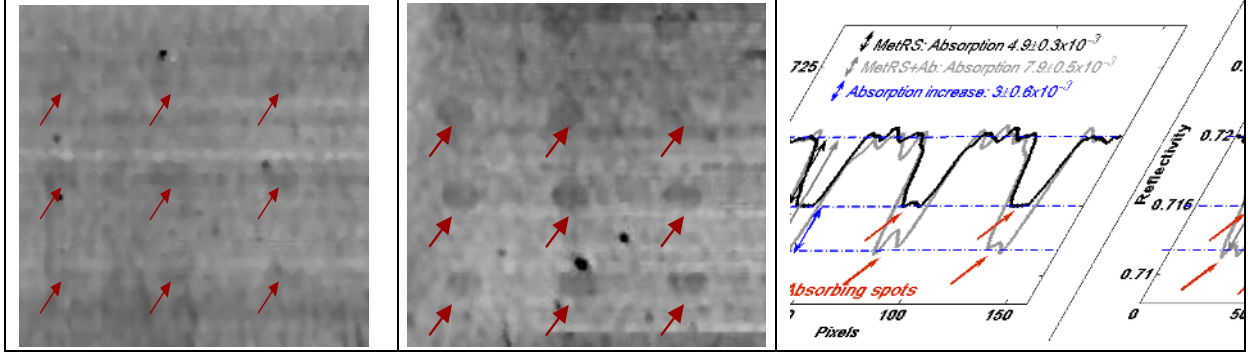


Figure 3: (a) and (b) UV images of a biochip coated with the MetRS protein before and after specific recognition with the anti-His Ab. Biological spots are indicated by arrows. (c) Reflectivity profiles on the biological spots line. The measured absorption is higher after specific recognition, due to the anti-His Ab absorption.

4. DESIGN OF CONTRAST ENHANCING GRATING BIOCHIPS

4.1 Contrast enhancement

We have seen that quarter-wave multilayer biochips offer a contrast enhancement of the order of 4, already sufficient to control biological coating and specific Ag/Ab coupling for monolayer density (typically 4×10^{12} molecules/cm²).

To be more sensitive, we use coupling properties of light obtained by structuration of the chip surface. This enables a largely enhanced light coupling (manifested classically by reflection anomalies, Fano shapes...) with the absorbing layer at the chip surface. The stronger interaction translates into a high enhancement of the absorption contrast. Contrast enhancing biochips are designed to enhance the interaction between the electromagnetic field and the absorbing layer. These chips consist in an ultraviolet mirror (aluminum $R_{Al,280nm} = 92\%$, or silicon $R_{Si,280nm} = 73\%$), covered with UV transparent dielectric (silica, silicon nitride, hafnium oxide, diamond...). The highest sensitivity occurs at resonance condition, given by equation (2) for grating structures of period Λ , where N is the effective index of the mode, θ_r the incidence coupling angle, and λ_r the resonance wavelength.

$$n_a \sin(\theta) = N(\theta_r) - m_g \frac{\lambda_r}{\Lambda} \quad (3)$$

4.2. Basics of coupling properties

In order to find a biochip structure which is highly sensitive to UV absorption, we determine the electromagnetic properties of our structure. We have to look here at the grating structure's resonant modes, i.e. those field that are self-sustained so that they acquire a large amplitude for the smallest excitation. The periodic geometry of the surface induces coupling between the different harmonics of a light wave. The resulting Bloch mode is a linear combination of in-plane harmonic waves:

$$E = \sum_G E_G(z) e^{i(k_{||} + G)r} \quad (4)$$

The coupling properties can for example couple well-sustained guided waves with waves leaking in air. Such configurations, if well exploited, reinforce the electric field in the absorbing layer, and consequently provide a stronger interaction. To know if a harmonic is diffracted to the ambient medium and available for external "pump" or "probe" actions, it is convenient to use the Ewald construction. For a harmonic of wavevector $k_{||}$, the diffraction condition to medium of index n_a is given by $|k_{||} + G| < n_a k_0$. When a harmonic meets this condition, it is propagative in the ambient medium and therefore diffract the Bloch mode's power in the ambient medium and can be used to image the chip.

Likewise, the harmonic can radiate to a medium of index n if $|k_{||} + G| < n k_0$. The Ewald construction therefore enables us to qualitatively see in which directions a Bloch mode energy is diffracted, or in which medium it is guided. To determine the sensitivity of our chip to a thin-absorbing layer on its surface, we need to determine the diffraction efficiency of the Bloch mode. This information can only be obtained by solving Maxwell's equations

and determining all the properties of the Bloch mode. For this, a scattering matrix formalism is used. The electromagnetic simulations of the code used here have been developed by A. David [[12]], and adapted to grating structures.

The solutions of the Maxwell's equations for grating with translational invariance along y can be classified in two families: TE and TM modes. In this paper, we only consider TE modes, which fulfil $\mathbf{E} = (0, E_y, 0)$, and $\mathbf{H} = (H_x, 0, H_z)$. The reflected energy corresponds to the flow of the Poynting vector emitted in the upward direction.

$$P = \frac{1}{2} \mu_0 c \int_{\Sigma_{up}} \text{Re}(E_{py} H_{pz}^* - H_{pz} E_{py}^*) \quad (5)$$

4.3 Biochip design

In this section, we describe the design of contrast enhancing biochips which will be used for imaging. The electromagnetic properties of our chip depend on its geometry and of the materials composing the chip. The layers parameters are the refractive index of the material composing it, their thicknesses, and the period of the corrugated layer. To determine the chip properties, we take into account the refractive index dispersions. For the UV mirror (aluminum or silicon), we use tabulated values [[13]], whereas for the dielectric layers (silica or silicon nitride), they are taken from our own ellipsometric measurements. For handiness of the experimental characterization, the first optimization is realized with air as an ambient medium.

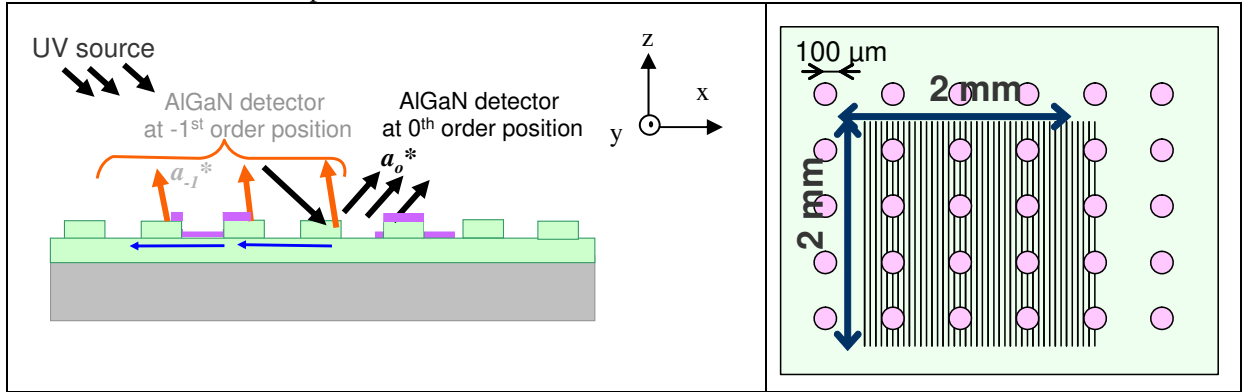


Fig. 4: Side view and top view of the fabricated biochip, composed of transparent dielectrics deposited on a UV mirror. The biochip diffracts several diffraction orders, whose diffraction efficiency will be affected absorbing molecules on its surface.

4.3.1 Transparent dielectric superposition

To confine the electric field at the chip surface, two transparent dielectric layers are deposited on a UV mirror. A higher interaction is obtained if the biological layer is coated on a guiding layer of high refractive index, in which the coupled wave is localized. In this paper, the biochip used is composed of a silicon nitride layer ($n \sim 2$) on a silica layer ($n \sim 1.5$).

4.3.2 Si “mirror” in UV

The reflectivity values of our aluminium substrate (83% at 280 nm) are lower than those found in tables (92%). Oxidation of the aluminium surface is suspected in this circumstance. Moreover, microscope imaging of the silica on aluminum biochip revealed that a large roughness appeared when silica was deposited, which induced a lower reflectivity. For these reasons, we prefer, for corrugated biochips, a silicon mirror (73% at 280 nm) instead of an aluminium one.

4.3.3 Designed structure

The biochip designed is therefore composed of a silicon reflector ($n_{280\text{nm}} \sim 1.86 + 4.49i$), covered with silica ($n_{280\text{nm}} \sim 1.5$) and silicon nitride ($n_{280\text{nm}} \sim 2$). The sum of the transparent dielectric thicknesses is close from quarter-wave thickness at the wavelength of interest. This enables us to take benefit from the factor 4 contrast enhancement as will be seen below. To model the sole absorption effect, the optical index of the absorbing layer is $1 + 0.02i$. The drawback of this assumption is that we do not take into account the phase shift induced by the biological layer. However, in water the optical index of proteins is close to the one of proteins “ambient medium”. The visible optical index of proteins is between 1.35 and 1.6. Thus, due to the phase difference, a shift towards higher wavelengths is expected. Consequently, to also take benefit of the real part of the effective index, we choose a

region were the optical index difference is favourable for our purpose. The optical thickness of the dielectric layers is slightly higher than quarter-wave thickness, so that we can take benefit of the reflectivity derivative $\partial R(\lambda)/\partial \lambda$ positive slope. Indeed, in this case, the shift towards higher wavelengths cause the reflectivity of the chip to be lower at a given wavelength λ_0 . Globally, it is seen to coincide with regions of relative minimum reflection, associated to the same enhancement as seen for the “specular” non corrugated biochip. The modes guided in silica and silicon nitride are indicated by arrows. The higher contrast enhancement occurs for the silicon nitride mode, which is more sensitive to the absorbing layer, since this latter is located on the silicon nitride surface.

4.3.4 Geometrical parameters

The diffraction direction of a diffracted order m depends on the material index and of the grating period. It is given by the classical grating equation:

$$n_m \sin(\theta_m) = n_0 \sin(\theta_0) + m2\pi/\Lambda \quad (6)$$

A simple representation of diffraction direction is this relation is the Ewald sphere. On the (θ, λ) reflectivity maps, we indicate lines corresponding to iso-diffraction angle of the -1st order, and the Littrow line (whereby $\theta_{-1} = \theta_0$). For imaging purposes, we are interested in diffracted orders emitted close from the sample normal.

We first presented above a selected successful case for heuristic purposes. We now come one step back and discuss the preferred values for all the parameters of the structure.

Obviously, a high index contrast between the top two layers enables a better confinement of the mode profile in the top layer, in contact with the biological element, and, thus, a higher contrast enhancement. Most of the high-index dielectrics tend to absorb UV light at the energetic wavelengths of 260-280 nm. Good candidates for high index materials are then silicon nitride ($n \sim 1.96$), hafnium oxide ($n \sim 2.1$) or diamond ($n \sim 2.42$). To take benefit of the large field of the fundamental harmonic the thicknesses of the dielectric layers are chosen to be close to quarter-wave thicknesses in the zone of interest. It could be thought in the first place that the resonant waveguide structure grants any desired strength of resonance, without such a need. However, notably because of the slightly absorbing mirror, the best use of the guided wave scattering into orders 0 and -1 occurs when the mentioned resonant condition is satisfied. In the simulations presented in Fig. 5, the real part optical index contrast is not considered, in order to really sense the absorption induced contrast. We will come back to this point in the next section, when discussing the experimental results. Concerning the grating mark-space ratio, the diffraction efficiency is not much affected in the range 0.35-0.65. The mark-space ratio also slightly changes the effective index of the guided wave. Concerning the sensitivity, it also depends on the ratio, not only through the variation of the harmonic profiles themselves, but also because those absorbing species lying in the bottom of the groove may experience a larger field amplitude than on the top of the teeth. However, it is to be noted that this effect can be mostly compensated by modulating the thicknesses of the transparent dielectric layers.

The etching depth directly controls the diffraction efficiency (photonic strength) and the width of the resonance. A high quality factor resonance leads to the highest sensitivity to a thin absorbing layer. However, the diffraction efficiency may then diminish. Moreover, as will be seen in the next subsection, when taking into account instrumental resolution, it is not necessarily profitable to have too sharp a resonance.

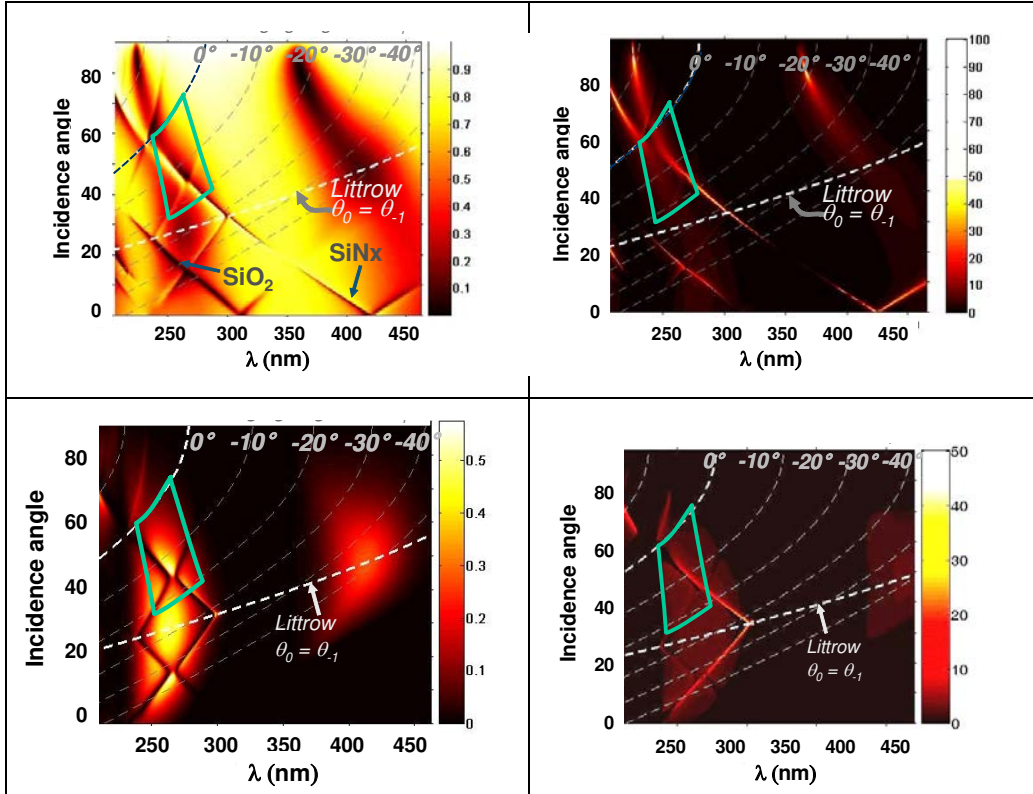


Fig. 5 : Reflectivity diagram in (θ, λ) in the 0^{th} and -1^{st} orders. The modes guided in silica and in silicon nitride are indicated by arrows. On the contrast map, we note that the mode guided in silicon nitride is more sensitive to the absorbing layer on its surface. The diffraction directions of the -1^{st} order are indicated by grey dotted curves. We also indicate the Littrow condition.

4.3.5 Guided modes

Concerning the guided mode in silica ($\lambda = 280 \text{ nm}$, $\theta = 7^\circ$), the electric field profile E_y of the harmonic $m=-2$ is a very wide guided wave located between silica and silicon nitride. The electric field of harmonic $m=0$ has roughly the same shape and periodicity as when the chip is not corrugated. Harmonic $m=-1$ electric field value is slightly lower than the one of the fundamental harmonic. Due to the diffracted direction, the period is shorter than for the fundamental harmonic. The next still noticeable harmonic is the $m=+2$ one. We note that it is the largest in the grating region, where it is fed by scattering of the fundamental harmonic $m=0$. Outside of the grating, it is evanescent and decays rapidly. It will interact with the biological layer and result in a decrease in reflectivity in the air diffracted harmonics.

Concerning the guided mode in the silicon nitride ($\lambda = 280 \text{ nm}$, $\theta = 40^\circ$), the harmonic $m=+1$ carries most of the mode energy. In comparison with the case where the structure is not corrugated, the fundamental mode (corresponding to the stationary wave in the absence of corrugation) is not much affected. The Ewald construction confirms that the $+1^{\text{st}}$ and -2^{nd} harmonics are guided in the silicon nitride, and will consequently interact much more with the absorbing layer on its surface. This is the reason why when looking at the absorption contrast with an absorbing layer is on the biochip, we have a large contrast enhancement for this mode.

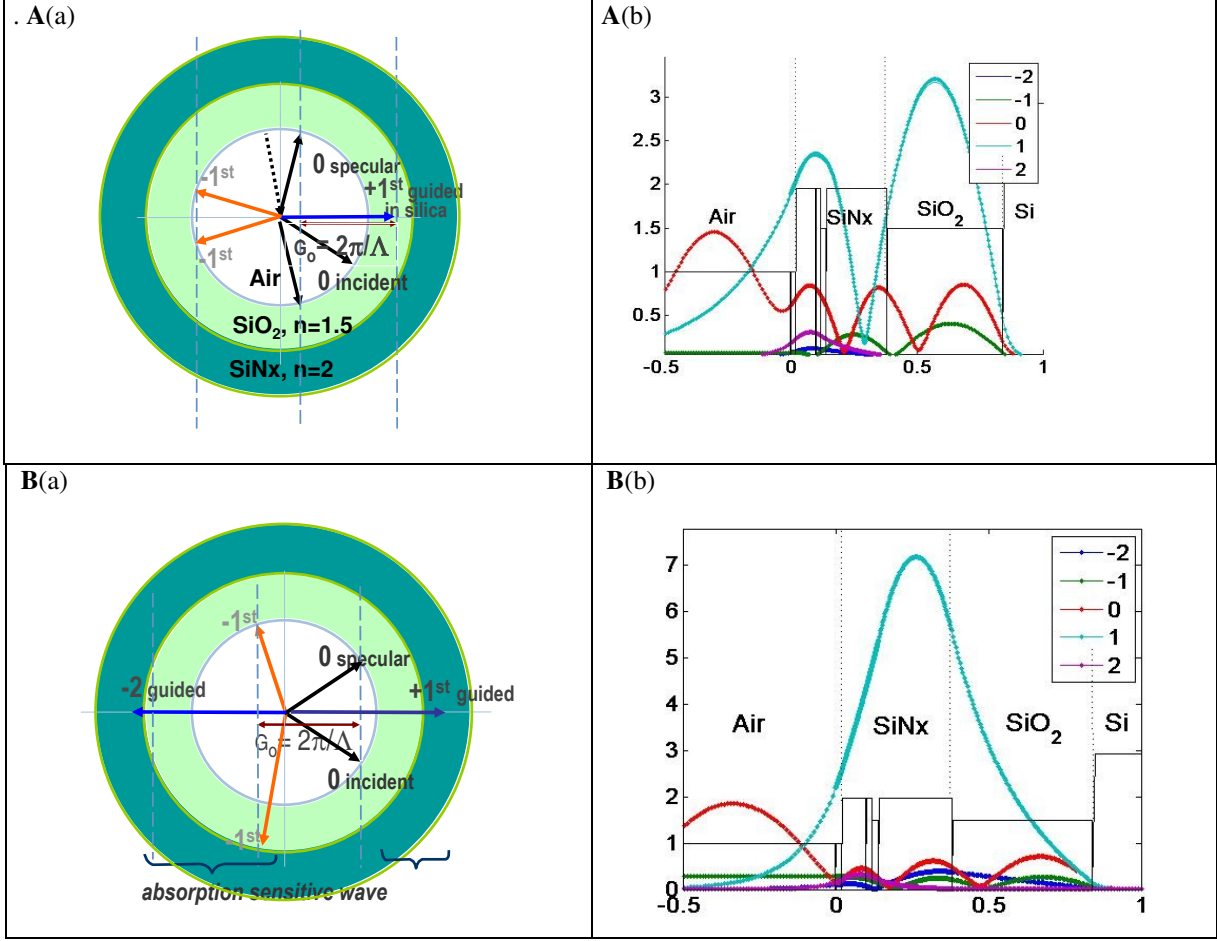


Fig. 6: Ewald construction and E_y component of the electric field for (A) the mode guided in SiO_2 and (B) the mode guided in SiNx .

4.3.6 Instrumental resolution limitations

To take into account the instrumental resolution, we convolve the reflected signal with spectral and angular resolution. For the 0^{th} order, the measured reflectivity is given by the following equation (6):

$$R_0 = R_0(\theta_r, \lambda_r)G(\theta)S(\lambda) \quad (6)$$

For the -1^{st} order, the diffraction direction, graphically given by the Ewald diagram, must also be considered. If operating at fixed incidence and detection angles, there is only a single point available on the reflectivity diagram (convoluted by the instrumental resolution). Thus, the reflected signal measured is also convoluted by a function $\delta(\theta, \lambda)$ corresponding to the diffraction directions collected by the detector.

$$R_1 = R_1(\theta_r, \lambda_r)S(\lambda)G(\theta)\delta(\theta', \lambda) \equiv R_1(\theta_r, \lambda_r)S(\lambda)G'(\theta, \theta', \lambda) \quad (7)$$

where the function $G'(\theta, \theta', \lambda)$ casts the way the variable-angle diffracted signal is captured by the instrument. It is particularly interesting, for imaging purposes, to detect the reflected signal close to the sample normal, so that the chip is in the object focal plane of the detector optics. Analysing the diffraction efficiency map, and the direction where the -1^{st} order is emitted, we note that some directions close to the sample normal also correspond to the silicon nitride guided mode, where the sensitivity to an absorbing layer is higher. This strongly suggests that it is possible to combine high sensitivity with good imaging properties.

In Fig 6 we give the diffracted spectrum for a given incidence angle for 0^{th} and -1^{st} orders for two different corrugation depths: $h_{\text{cor}} = 14 \text{ nm}$ and $h_{\text{cor}} = 28 \text{ nm}$. For the -1^{st} order, the presented result of the calculation implicitly tracks the angle associated to each wavelength. We provisionally neglect the imaging issues caused by the grating chromatic dispersion (typically spreading light over 3° for a 10 nm span here).

We consider two different spectral resolutions: the one corresponding roughly to a laser illumination, and the one corresponding to a LED and/or a spectrally selective AlGaIn detector associated with a spectrally broader source.

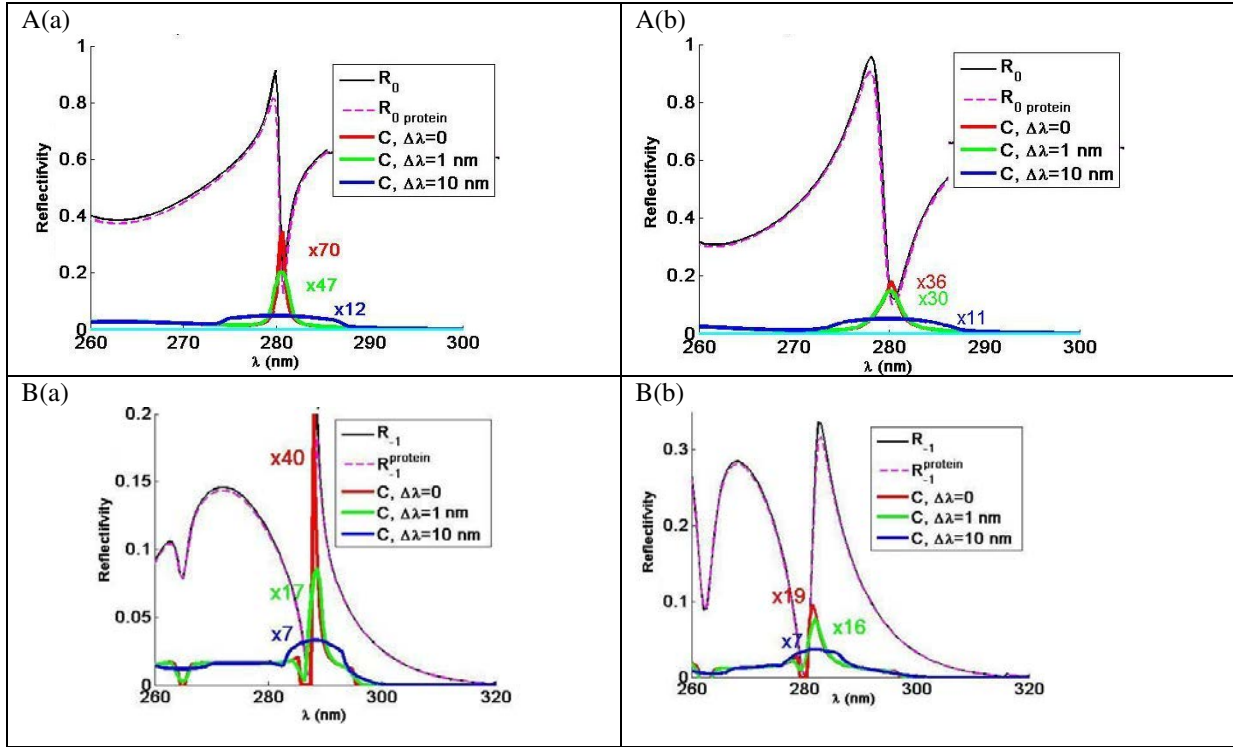


Fig.7: Reflectivity profile in the order 0th -1st, for two different corrugation thicknesses: $h=14$ nm, and $h = 28$ nm.

For a corrugation thickness of 14 nm, for the 0th order, the contrast enhancement at 280 nm is 70 if not taking into account the spectral resolution, 40 for a resolution of $\Delta\lambda \sim 1$ nm, and 12 for a resolution of $\Delta\lambda \sim 10$ nm. Concerning the -1st order, the measured signal corresponds to the one diffracted in the direction of detector, and is less influenced by the spectral resolution. For a spectral resolution $\Delta\lambda = 1$ nm, the contrast enhancement decreases from 40 to 17 for a corrugation thickness of 14 nm, and from 19 to 16 for a corrugation thickness of 28 nm. From these diagrams, we see that the diffraction efficiency in the -1st order is lower when the corrugation thickness is of 14 nm. Thus, we are more interested in the grating etched of 28 nm, since it gives us a similar sensitivity when taking into account the instrumental resolution, with a higher signal level.

5. EXPERIMENTAL RESULTS

5.1. Chip fabrication and preparation

Our chip is composed of a silicon mirror, covered with transparent dielectrics: silica ($n \sim 1.5$) and silicon nitride ($n \sim 2$). The total optical thickness of the transparent dielectric layers is $\lambda/4$, so that the field of the stationary wave is maximal on the interface. The optimal biochip presented above consisted of a silicon mirror, covered with a silica layer of thickness 140 nm, and a silicon nitride layer of thickness 78 nm, with a period $\Lambda = 280$ nm. Both the silica and silicon nitride are deposited by PECVD (Plasma-enhanced chemical vapor deposition) at 340°C. The thickness and refractive index dispersions of the layers are next determined by ellipsometry. Then, structuration of the chip surface is carried out using electron-beam lithography. The silicon nitride is etched using a RIE (reactive-ion etching) process. For compatibility with our biological coating process, a very thin silica layer (~ 3 nm) is deposited on the biochip prior to biological coating. The silicon nitride thickness is of 90 nm, and the thin silica thickness is 3 nm. The etching depth is determined by ellipsometry measurement of a witness sample. Its depth is about 22 nm.

5.2 Spectro-angular properties characterization

5.2.1 Goniometric set-up

Figure 8 gives a scheme of the set-up used to characterize nano-structured chip. It is composed of a Xenon continuous source, illuminating a sample with collimated illumination and placed on a θ - 2θ goniometer. The angular resolution of the illumination is 1.5° . The reflected signal is measured with an Opton-300i spectrometer with optical UV fiber provided from OceanOptics. To normalize the signal, we first measure the illumination spectrum transmitted through the optical fiber by aligning the fiber to the illumination axis at 180° .

To determine the sensitivity to biological absorption, two nominally identical gratings are fabricated on the same chip, and one of them is fully covered with a monolayer of the MetRS protein. Measuring the two reflectivity maps, we can thus compare the diffraction efficiency of the biochip with and without biological absorber on its surface. The two spectro-angular diffraction efficiency maps $R_j(\theta, \lambda)$ are measured successively, by translating the chip using an electric translation stage between the two measurements, so that optical settings are quasi identical for the two measurements. The two gratings being on the same chip, most spurious contributions which could influence the contrast (fabrication reproducibility and also optical settings) are limited.

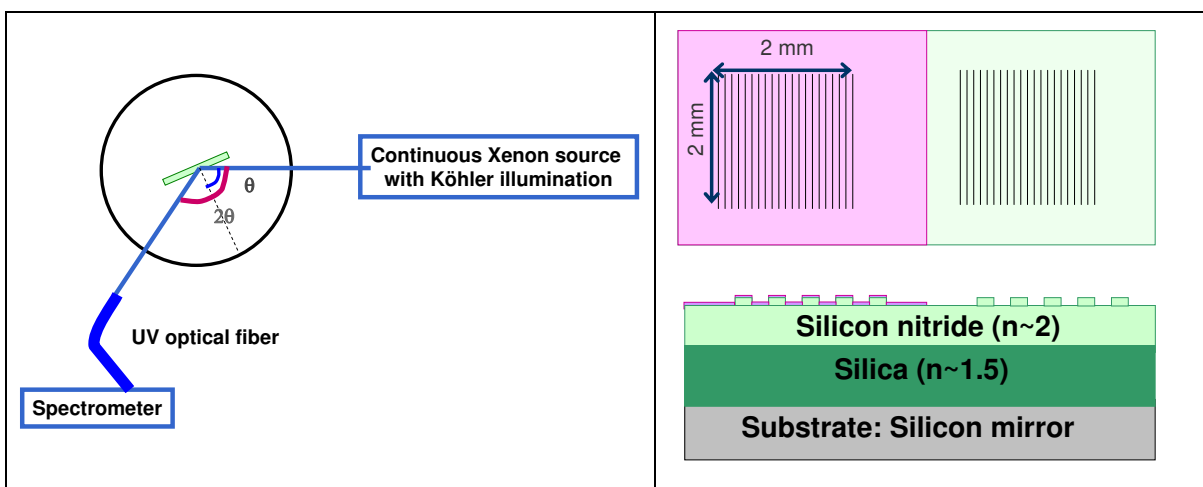


Fig. 8 (a) Set-up used to characterize spectrally and angularly the chips fabricated. The sample is placed on a θ - 2θ goniometer, illuminated with a collimated beam. (b) Spectrum acquired at an incidence angle of 40° . The entire map is acquired by successive acquisition when changing the incidence angle with the goniometric set-up

5.2.2 Spectro-angular reflectivity measurements

In figure 9, we give both the simulated reflectivity diagram and the corresponding $R_o(\theta, \lambda)$ experimental measurement. The two maps are in very good agreement concerning all singularities positions, signs, and all smooth trends. Most strikingly, we clearly see the mode guided in the silicon nitride and the one guided in silica. In comparison with the parameters of the chip presented above, the fabricated chip silica thickness is 130 nm ; consequently, to keep the total dielectric similar to the structure presented in the previous section, the silicon nitride deposit was of larger thickness. This difference slightly diminishes the contrast enhancement: the larger silicon nitride layer results in a less confined mode, and diminishes the interaction with the absorbing layer.

In figure 9, we give both the simulation of the reflectivity diagram and the experimental measurement. These maps are in good agreement. Since the measurements are realised in air as an ambient medium, we predominantly observe a shift towards larger wavelength (about 2 nm). Consequently, it is not possible to determine here the contrast enhancement that will be obtained for our chip in water. Moreover, even though the gratings with and without biological layer are located on the same chip, and the translation is carried out with a motorized translation stage, we cannot grant a completely perfect absence of optical settings modifications. Thus, only imaging results will give us an accurate improvement in sensitivity. Diffraction efficiency of the -1st

order is not trivial, since at a given incidence angle, the detector must be at the diffracted angle position for a given wavelength. This measurement can be carried out using a set-up following the $\sin(\theta_i)$ relation. Our chip characterization realised for the specular reflection informs us about the diffraction efficiency and gives a good insight in the reflectivity diagram by performing simulations in parallel. but even with fitted simulations, the accurate contrast enhancement obtained in the -1^{st} order may only be determined from imaging experiments.

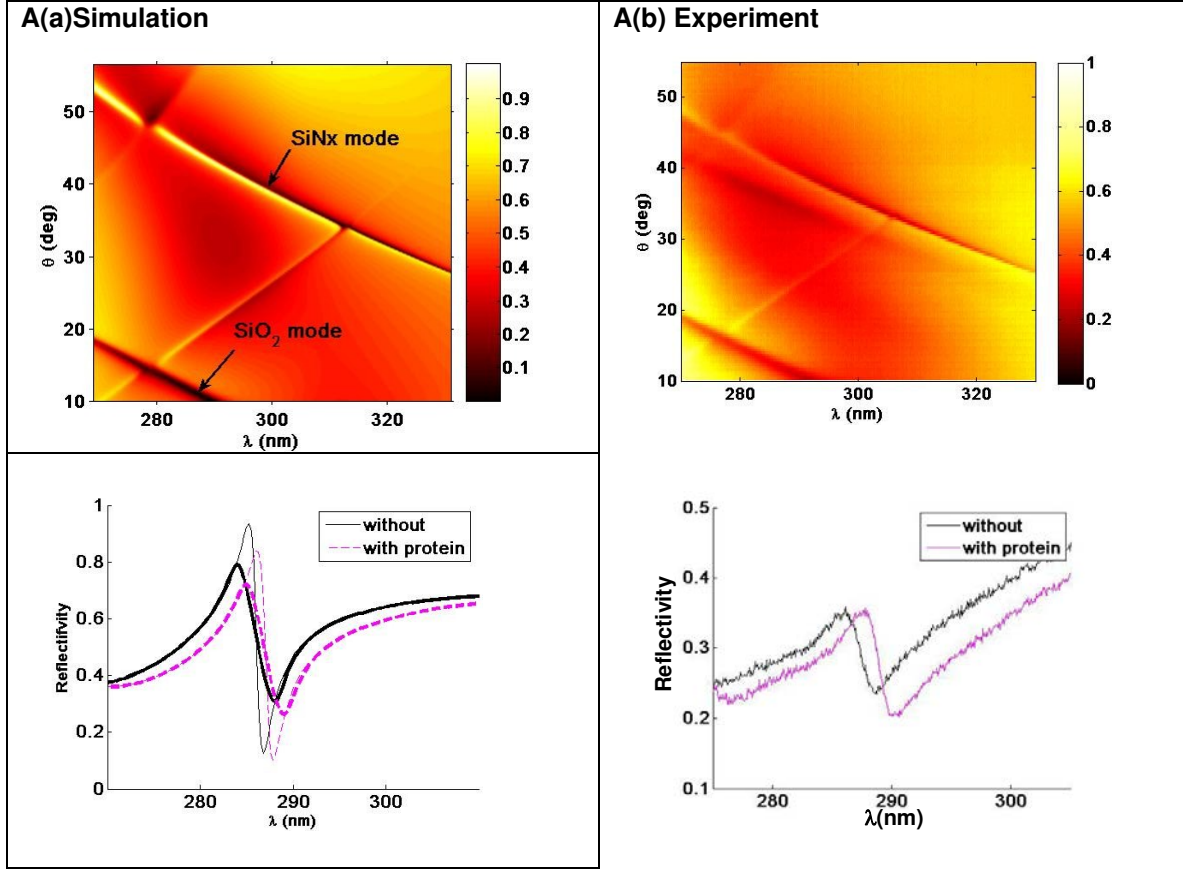


Fig. 9 (a) Simulated and (b) experimental reflectivity diagram of the chip in the 0^{th} order. In the simulation, the optical index of the protein layer is taken to $1.4+0.02i$. The real part of the optical index causes a shift of the reflectivity spectrum towards high wavelengths.

6. CONCLUSION AND PERSPECTIVES

6.1 Contrast enhancement with multilayers and with grating biochips

In this paper, we have presented design, fabrication and characterization of biochips developed for UV imaging for label-free biodetection. These biochips aim at enhancing the absorption induced contrast when a UV absorbing monolayer, or less, is present on their surface. First, multilayer biochips offering a contrast enhancement of a factor of the order of 4 have been presented. This sensitivity is sufficient for applications such as coating control and detection of specific recognition for high molecular probe density (typically 4×10^{12} molecules/cm²), corresponding to a sensitivity in the ng/mm² order. To obtain a higher contrast enhancement, we develop reflective grating biochips, which exploit confined light-matter interaction, and thus enable a higher contrast enhancement. A contrast enhancement of 70 can be obtained in the 0^{th} order, whereas this contrast enhancement is of 40 in the -1^{st} order, this latter being close to normal incidence. Taking into account instrumental resolution ($\Delta\lambda=1\text{nm}$, and $\Delta\theta=1.5^\circ$), we have seen that these values reduce to 30 and 16 respectively. This corresponds to sensitivity of a few tens pg/mm² for proteins, and of the order of only a few pg/mm² for DNA. This validates the potential of our method in the field of biodetection.

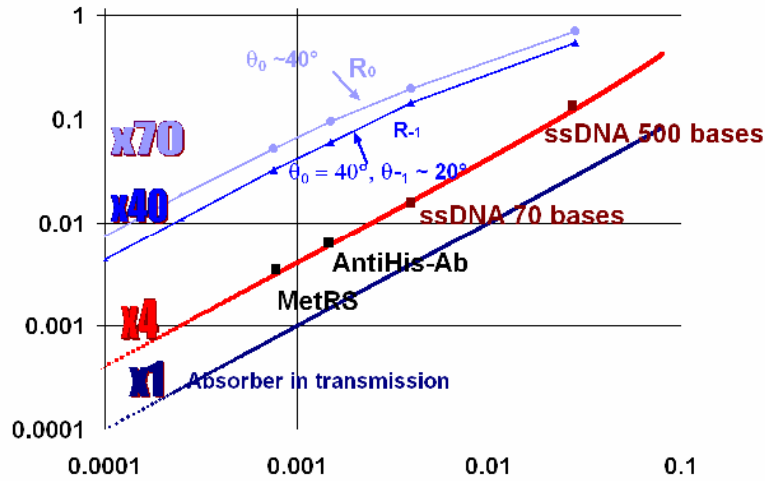


Fig. 10: Contrast enhancement in log-log scale, in comparison to the transmission contrast.

6.2 Perspective for sensitivity enhancement

Two direct perspectives are foreseen to make our biochip more sensitive. First, the materials used here are silica and silicon nitride. Advantages of these materials are their UV transparency. Its low optical index and its common use of silica make it a good candidate for the bottom cladding material. Concerning the high index materials, other choices are possible. Among them, we find diamond ($n_{280\text{ nm}} \sim 2.42$), hafnium dioxide ($n_{280\text{ nm}} \sim 2.1$) and a couple of less common oxides and nitrides... Silicon nitride was chosen because of its availability in our clean room. However, transparent materials of higher index would be better candidates to enhance the contrast. Moreover, in the simulation presented here, the ambient medium is air, which was easier to establish the first relevant spectral measurements. When our biochip will be in water, the interaction can be enhanced because the antinode of the silicon nitride guided mode will come closer to the interface with water whose UV index $n \sim 1.39$ than it does in air.

6.3 Imaging of grating biochips

While the absolute diffraction efficiencies have their own interest, it remains to be established that large signals are equally obtained in imaging conditions, with enough signal, low enough aberrations. Although the contrast enhancement may probably be still increased, we stress that, for protein detection, the sensitivity readily obtained experimentally is on the order of the ng/mm^2 . With grating structures, we expect it to attain tens of pg/mm^2 , and thus few the pg/mm^2 for DNA, since DNA absorption is ten times higher than that of proteins for a given areal mass coverage.

REFERENCES

- [1] Gauglitz, G., "Label-free optical biosensors", *Proc. EOS Annual Meeting 2008* (2008).
- [2] Fasman, G.D., "Handbook of Biochemistry and Molecular Biology, vol. I.", CRC. Press, Cleveland, OH. (1975)
- [3] Cassio, D., Waller, J.P., "Modification of methionyl-tRNA synthetase by proteolytic cleavage and properties of the trypsin-modified enzyme", *Eur. J. Biochem.* 20 (2), 283–300 (1971).
- [4] Reverchon, J.L., Robot, J.A, Truffer, J.P., Caumes, J.P., Mourad, I., Brault, J., Duboz, J.Y. , "AlGaIn-based focal plane arrays for selective UV imaging at 310nm and 280nm and route toward deep UV imaging", *Proc. SPIE*, Vol. **6744-9** (2007).
- [5] CryLaS GmbH, www.crylas.de/
- [6] Clampin, M., "Ultraviolet-optical charge-coupled devices for space instrumentation", *Opt. Eng.*, **41**(6), pp. 1185-1191 (2002)
- [7] Bai, Y., Bernd, S.G., Hosack, J.R., Farris, M.C., Montroy, J.T., Bajaj, J., "Hybrid CMOS Focal Plane Array with extended UV and NIR Response for Space Applications", *Proc. SPIE* **5167**, pp. 83-93 (2003).
- [8] Saint Pe, O., Astrophysics Detectors Workshop, Nice (2008).
- [9] Lindler, M., Elstein, S., Panitkova, E., Permuter, B., Lindker, P., "UV devices for solar blind & background limited detection", *Proc. SPIE* **3110**, pp. 527-534 (1997).
- [10] Shur, M.S., Gaska, R., "III-nitride based deep ultraviolet light sources", *Proc. SPIE* **6894**, pp. 689419-8 (2008).
- [11] Robin, K., Reverchon, J.L., Mugerli, L., Fromant, M., Plateau, P., Benisty, H., "Detection of biological macromolecules on a biochip dedicated to UV specific absorption", *Bios. Bioelec.*, in press, available online, doi:10.1016/j.bios.2008.08.028 (2008).
- [12] David, A., Benisty, H., Weisbuch, C., "Optimization of Light-Diffracting Photonic-Crystals for High Extraction Efficiency LEDs", *J. Display Technol.* **3**, pp. 133-148 (2007).
- [13] Palik, E.D., "Handbook of Optical Constants of Solids", Academic Press Inc. (1985).
- [14] Rosenblatt, D., Sharon, A., Friesem, A.A., "Resonant grating waveguide structures", *IEEE J. Quant. Electron.*, 33(11), pp. 2038-2059 (1997).